Generation of gamma ray beams with tunable energy by annihilation of positrons in flight*

R. J. Abrams[1], A. Afanasev[1, 2], C. Ankenbrandt[1], K. Beard[1], S. A. Bogacz[3], L. Campbell[4], J. E. Fast[4], G. Flanagan[1], R. P. Johnson[1], D. Neuffer[5], M. Popovic[5], and C. Yoshikawa[1]

[1]*Muons, Inc., Batavia IL, USA*

[2]*Hampton University, Hampton, VA, USA*

[3]*Thomas Jefferson National Accelerator Facility, Newport News, VA, USA*

[4]*Pacific Northwest National Laboratory, Richland, WA, USA*

[5]*Fermilab, Batavia, IL, USA*

(Received April XX, 2011)

Design concepts are presented for a system to produce beams of nearly monoenergetic gamma rays tunable in an energy range around 10 MeV. The gamma rays are produced in the forward direction by annihilation in flight of nearly monoenergetic positrons. The positrons are produced by an electron beam impinging on a target subsystem optimized for positron production within the acceptance of the downstream subsystems. The target is followed by an innovative "dipole plus wedge" monochromator, in which the positrons are bent 180° in a uniform magnetic field to disperse their momenta, after which a wedge absorber selectively reduces their momentum spread to a narrow range. Those positrons then impinge on a low-Z converter plate in which some of them annihilate with atomic electrons in the converter to produce the desired gamma ray beam. Simulations using G4Beamline (which in turn uses Geant4) have been performed to verify the concepts and to evaluate the system performance.

DOI: 10.1103/PhysRevSTAB.NN.nnnnn PACS numbers: 41.85.Si, 25.30Hm, 25.30.Rw

I. INTRODUCTION

Beams of nearly monoenergetic gamma rays tunable in the energy range around 10 MeV are useful for research and for a number of industrial applications. One such application, of primary interest here, is for scanning of cargo for fissionable materials by inducing photofission reactions in those materials, which then are identified by detection of the delayed fission neutrons or gammas as a telltale signature of their presence [1]. The ideal system would provide an intense, nearly monoenergetic gamma ray beam that can be tuned to the energies of interest. In practice, an energy spread of about 1 MeV is small enough because photofission of actinide nuclei proceeds through a giant dipole resonance that is fairly broad [2].

The most common method of producing beams of high-energy photons is by bremsstrahlung of energetic electrons passing through a high-Z target. Bremsstrahlung beams can be intense, but there are two disadvantages. First, the resulting spectrum of photons is too broad, and the photon flux, which falls roughly as $1/E_\gamma$, provides a large excess of unwanted photons at energies below photofission thresholds.

This results in high radiation doses to the interrogated targets and surrounding areas, higher backgrounds, and possible pileup effects in detectors. Second, the bremsstrahlung spectrum is suppressed toward its high-energy endpoint. Therefore in order to produce high fluxes of energetic photons, one

* This work was funded by Pacific Northwest National Laboratory which is operated for the U.S. Department of Energy by Battelle Memorial Institute under Contract DE-AC06-76RLO 1830.

needs to produce photons above the desired energy, which leads to additional unwanted effects such as residual radioactivity of the scanned targets.

The method described here is to produce nearly monoenergetic gamma rays by annihilation of nearly monoenergetic positrons. The positron energies can be tuned, and the energies of the produced gamma rays can therefore be adjusted. The principle of using positron in-flight annihilation as a source of monoenergetic photons is not new. In fact, such sources successfully operated in the past in LLNL [2] and Saclay [3], and produced a large amount of high-quality data on photonuclear reactions [4,5]. The objective of the work reported here is to design a new generation of operationally robust positron-based gamma sources that can provide the high intensities needed for applications. Besides advancing technologies for nuclear non-proliferation, the proposed high-flux gamma source may be useful for fundamental studies of photonuclear reactions.

The next section presents an overview of the proposed system. The following three sections describe the positron production subsystem, the positron "dipole plus wedge" monochromator, and the conversion of the positrons into nearly monoenergetic photons.

II. SYSTEM OVERVIEW

The overall system, shown conceptually in Fig. 1, includes three major subsystems. In the first subsystem, an electron beam of about 75 MeV from an accelerator (not shown) impinges on a high-Z target to produce the positrons. In the second subsystem, a dipole-plus-wedge monochromator creates a nearly monoenergetic positron beam in the following manner. Positrons produced in the high-Z target are bent 180° and momentum-dispersed in the first dipole magnet, so that their momenta are linearly correlated with their horizontal position along the face of the wedge. The positrons pass through the wedge ionization energy loss absorber, such that their energies become concentrated near a single value. Because the dipole magnet disperses according to momentum we use momentum as an attribute of the positrons. Our simulations show that a linearly increasing wedge thickness results in momenta concentrated after the wedge within the precision of the simulations. In the third subsystem, the resulting nearly monoenergetic positrons are bent in the second dipole magnet to impinge on a fixed target of low-Z material in which some of them convert into a nearly monoenergetic beam of gamma rays via in-flight annihilation on the electrons in the target.

Note that this configuration provides several beneficial effects:

- Electrons produced in the high-Z target are swept in the opposite direction to the positrons, thus reducing the contamination of the positrons;
- High energy electrons (E ~75 MeV) that emerge from the target are deflected much less than the positrons of interest (E ~ 10 MeV) in the dipole magnet and pass out of the rear of the dipole magnet into a beam dump (not shown);
- Protons and other heavy positive particles emerging from the target and impinging on the wedge lose more energy than positrons and are absorbed in the wedge.

The simulations presented here are optimized to produce nearly monochromatic gamma-ray beams with energies around 10 MeV. This choice of energy is application-driven: it is optimized for detection of fissile materials while minimizing the induced radioactivity in the scanned objects. However, the same system can be tuned to produce gammas at other energies as needed. Additionally, the system described throughout this paper is intended to be field-deployable.

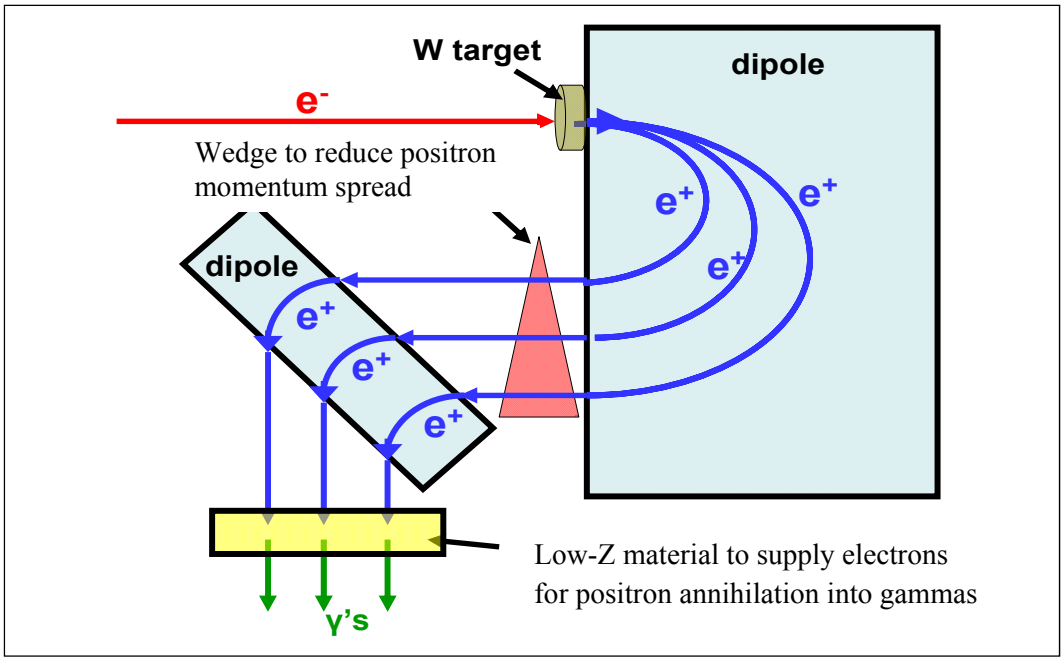

FIG. 1: Conceptual design of the system for producing nearly monoenergetic photons.

III. POSITRON PRODUCTION

The positron production subsystem needs to produce a high yield of useful positrons while remaining compact enough to be field-deployable. Additionally, the subsystem must satisfy the requirements of the downstream subsystems, primarily the dipole-plus-wedge monochromator. In particular, the monochromator works well for positrons produced within about 300 mr of the forward direction in a small source region at the entrance of the dipole. Useful positrons are defined as those emanating from a small source region with energies in the desired range and production angles less than 300 mr.

Tungsten (W) was chosen as the target material because it has the highest melting point of readily available high-Z materials and is a common choice for positron or photon production by an electron beam. High-Z targets are favored because they generate more bremsstrahlung gammas than low-Z targets and convert them more efficiently into electron-positron pairs. Furthermore, their small radiation length limits the spatial extent of the positron source region.

Two simple target shapes were considered: a thin wire and a large-radius circular disk (effectively a slab). Although more positrons are produced from a wire because many positrons escape from the sides of the target, a disk shape was chosen for the subsequent analysis described here because more positrons are produced within 300 mr of the forward direction in that case. (Preliminary results suggest that targeting the electrons on the edge of a thin circular disk in the median plane of the dipole will provide somewhat higher yields; engineering considerations that are beyond the scope of this paper will affect the final choice of target configuration.)

The electron beam energy and the target thickness were chosen by adjusting those two parameters to optimize the yield of useful positrons per unit electron beam power, taking into account also the production rate of unwanted background neutrons. This procedure resulted in the choice of electron beam energy of 75 MeV and target thickness of 4.4 mm. These values are used in the subsequent calculations and simulations presented in this paper.

For additional discussion of the positron production subsystem, see IPAC10 [6].

IV. POSITRON MONOCHROMATOR

A. Concept

The dipole-plus-wedge monochromator provides the ability to vary the energy and greatly reduce the momentum spread of the positron beam. This in turn enables a nearly monoenergetic and tunable photon beam to be produced from the conversion target [7]. A schematic representation of the operating principle is shown in Fig. 2. The basic idea behind the dipole-plus-wedge scheme is that:

1. Positrons produced near the forward direction with a given momentum in a uniform dipole field converge after a 180 degree bend to a horizontal focus.

2. The positions of these horizontal foci are dispersed in momentum, with higher momentum positrons farther from the production target.

3. A wedge-shaped energy absorber can be placed such that each positron will be left with approximately the same momentum after it passes through the absorber. This will produce a wide, nearly monoenergetic positron beam.

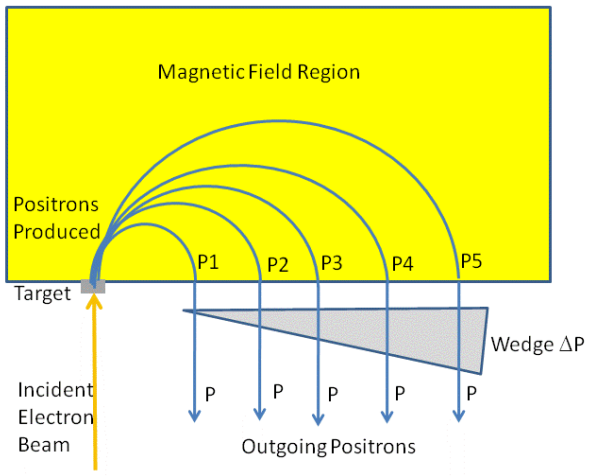

FIG. 2. Illustration of dipole-plus-wedge monochromator concept. Outgoing positrons emerge with momentum P, which is essentially equal to P1, the lowest momentum passing through the tip of the wedge.

An additional important feature of this design is the suppression of large backgrounds by incorporating a large bend angle. Shielding can also be incorporated around the dipole and in the gap, and the pole tips themselves provide shielding. In addition to suppressing the backgrounds, this design has the additional advantage that the positrons are captured from the phase-space region with the largest flux.

In order to achieve a system that is momentum-tunable, one can set the magnetic field appropriately for each desired momentum and use a wedge with the appropriate angle for that case. For example, in order to provide a 10 MeV/c beam, one can take all of the positrons produced with momenta between 10 MeV/c and about 20 MeV/c and use the appropriate dipole field and wedge taper to reduce the momentum spread and provide a nearly monoenergetic beam at 10 MeV/c.

Details on the following simulation studies and results are presented in this section:

- Selection of beryllium (Be) as wedge material;
- Performance of dipole and wedge for 2 MeV/c, 5 MeV/c, and 10 MeV/c positrons;
- Study of performance of dipole plus wedge using a simulated realistic sample of positrons produced by a beam of 75 MeV electrons bombarding a 4.4 mm thick tungsten target. Yields per

incident electron and RMS values of momentum spread after the wedge are reported for 2 MeV/c, 5 MeV/c, and 10 MeV/c final momenta.

- Dependence of positron yield, momentum spread and angular spread on maximum positron production angle.
- Comparison of the performance of a dipole-plus-wedge with that of a dipole plus a collimator.

The dipole and wedge layout for a simulated idealized positron beam consisting of 3 discrete momenta at normal incidence is shown in Fig. 3.

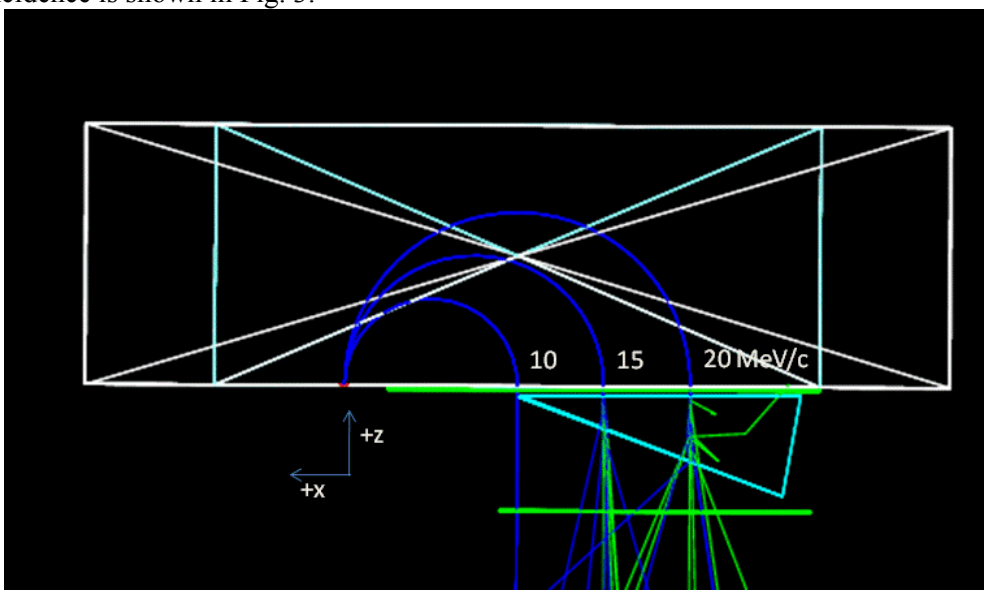

FIG. 3. G4beamline [**8**] simulation display of trajectories of an ideal beam of mixed momenta (10 MeV/c, 15 MeV/c, and 20 MeV/c) at normal incidence in a uniform magnetic field. Beam particles are shown to pass through a Be wedge. Positron trajectories are shown in blue, gammas produced in wedge are shown in green.

The trajectories are semi-circular and emerge as 3 separate beams. The figure shows trajectories for 5 beam particles at each momentum. The wedge shown is Be and is designed to reduce all of the outgoing momenta to 10 MeV/*c*, a nearly monoenergetic beam. Scattering of the positrons in the wedge is as indicated for the small random sample of trajectories shown.

For a positron of a given momentum produced with a non-zero production angle at the face of a uniform dipole, it can easily be shown that the horizontal displacement at the dipole exit is proportional to the cosine of the projected horizontal production angle. Furthermore, the exit angle is the same as the entrance angle. Positrons produced out of the x-z plane are limited to a vertical angular range determined by the dipole magnet gap. The extra component of vertical momentum for these positrons largely compensates for the longer path length and extra energy loss that they have in passing through the wedge with a vertical angle. The empirical method used to determine the optimum wedge dimensions is described in Appendix B.

B. Results for positrons produced by 75 MeV electrons on tungsten target

The dipole-plus-wedge performance was studied using the sample of positrons generated at the output of the optimized electron beam-W target configuration described in the previous section. The optimized positron production subsystem was comprised of 75 MeV/c electrons on a W target 4.4 mm thick. An

input collection of positrons was generated with $1x10^6$ electrons on target. The configuration used to study the dipole plus wedge performance is shown in Fig. 4. Shielding blocks were added to reduce the number of stray particles that hit the virtual detector (represented as a green rectangle).

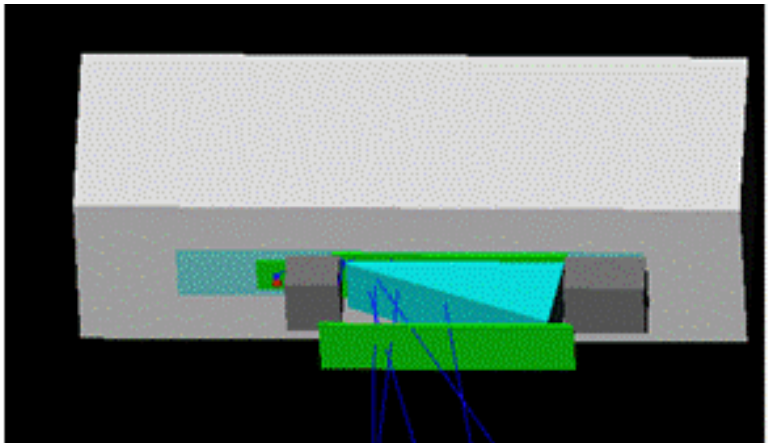

FIG. 4. Test Layout: Dipole and Wedge; Pb shielding blocks along magnet gap are in dark grey, virtual detectors are in green, beam tracks originate at the red dot.

Combinations of dipole fields and corresponding wedges were studied for three final momenta: 2 MeV/c, 5 MeV/c, and 10 MeV/c. The 10 MeV/c case is the one of most interest for generation of gamma rays for the photofission application.

The performance of the dipole and wedge is illustrated for the 10 MeV/c case in Fig. 5. The positron momentum distribution before the positrons hit the wedge, shown in Fig. 5 (top), has a broad spectrum, extending up to about 30 MeV/c, with a mean momentum of 9.4 MeV/c, an RMS of 5.6 MeV/c, and an asymmetrical shape. The final momentum distribution, after positrons emerge from the wedge, is shown in Fig. 5 (bottom). The resultant distribution is narrowed to a nearly monoenergetic peak, with a FWHM of ~2.4 MeV/c, corresponding to an RMS spread of ~1 MeV/c, or ~10%. The low momentum tail can be further suppressed by improvements to the shielding.

Plots of x-position versus momentum before and after the wedge are shown in Fig. 6 (top and bottom), which shows how the final distribution is improved by the wedge.

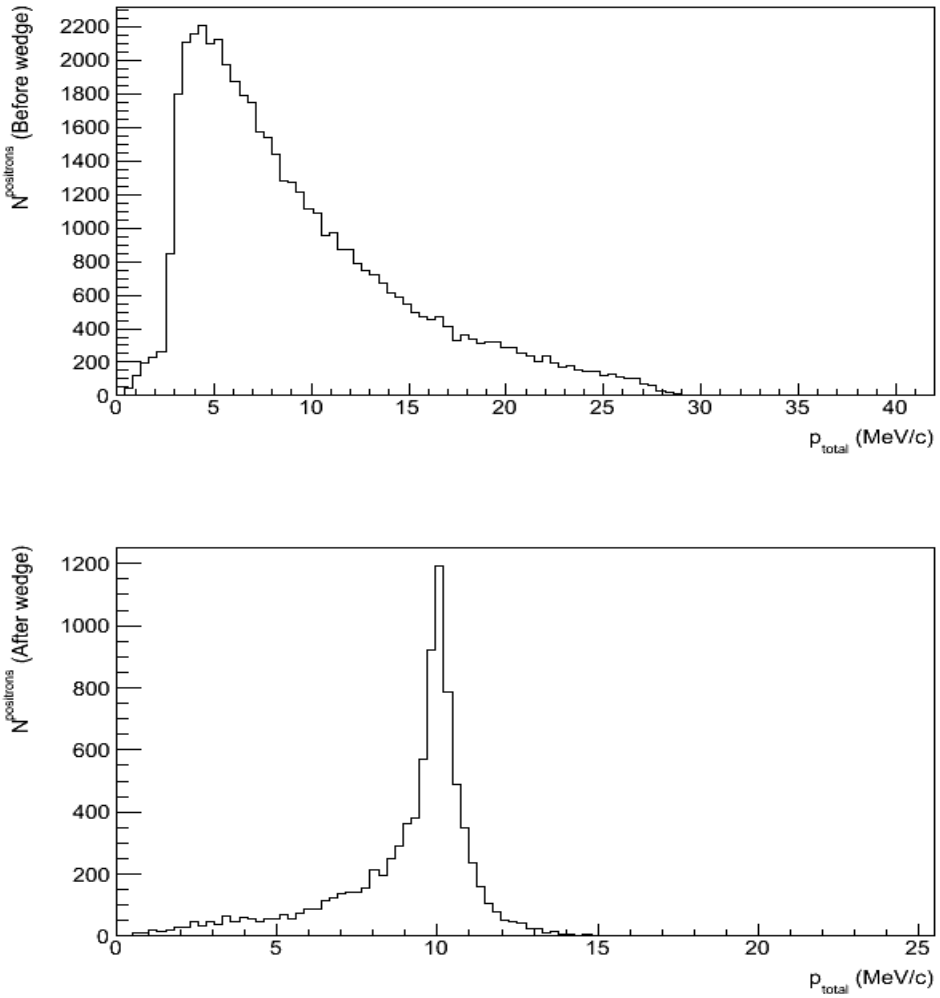

FIG. 5. Momentum spectra of positrons before (top) and after (bottom) 10 MeV/c wedge.

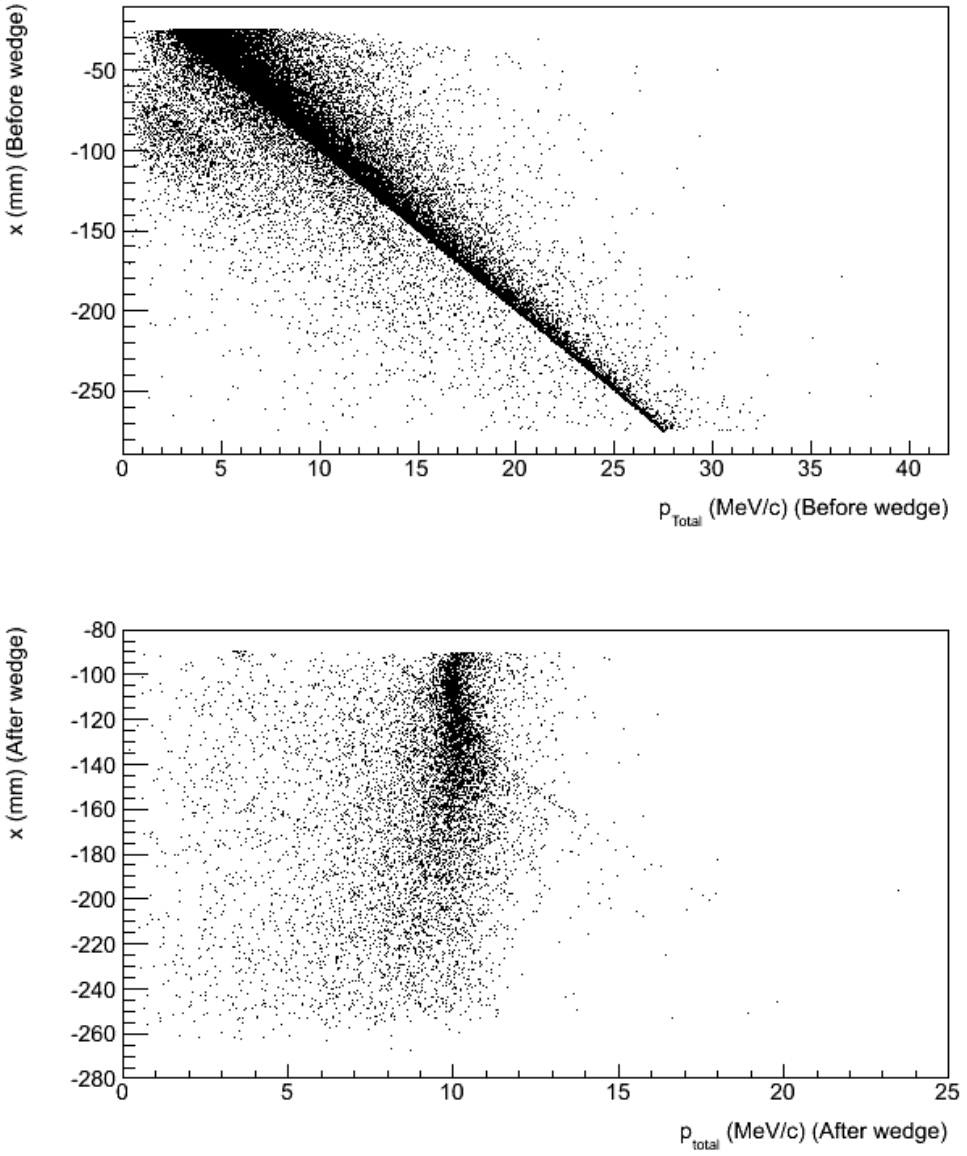

FIG. 6. Scatter plot of x-position vs momentum before (top) and after (bottom) 10 MeV/c wedge.

Summary of Results for 2, 5, and 10 MeV/c Final Momenta

Similar computations were performed with wedges designed to produce either 2 MeV/c or 5 MeV/c momenta. The momentum peak sharpens with increasing momentum, and the angular spread is nearly independent of momentum. Results for 2 MeV/c, 5 MeV/c, and 10 MeV/c are shown in Table 1.

Table 1: Momentum peak, angle, and number of surviving positrons for 2, 5, and 10 MeV/c dipole and wedge combinations. All yields are based on 10^6 electrons on the same W target.

P_{Final} (MeV/c)	P_{RMS}/P_{Final} (%)	Θ_{RMS}(°)	# e^+ After Wedge (Y_{Wedge})
2	15	17	2961
5	8	18	12180
10	4	23	8963

A. Effects of restriction of positron production angle

The analysis in Section A suggests that collimating to restrict the production angles of the positrons can lead to more sharply defined momentum peaks after the positrons pass through the wedge. The results of applying cuts to the tangent of the positron production angle in the x-z plane are shown in Fig. 7. The momentum distributions and the angular distributions after the wedge become narrower as the cuts are made more restrictive. A summary of the results is shown in Table 2.

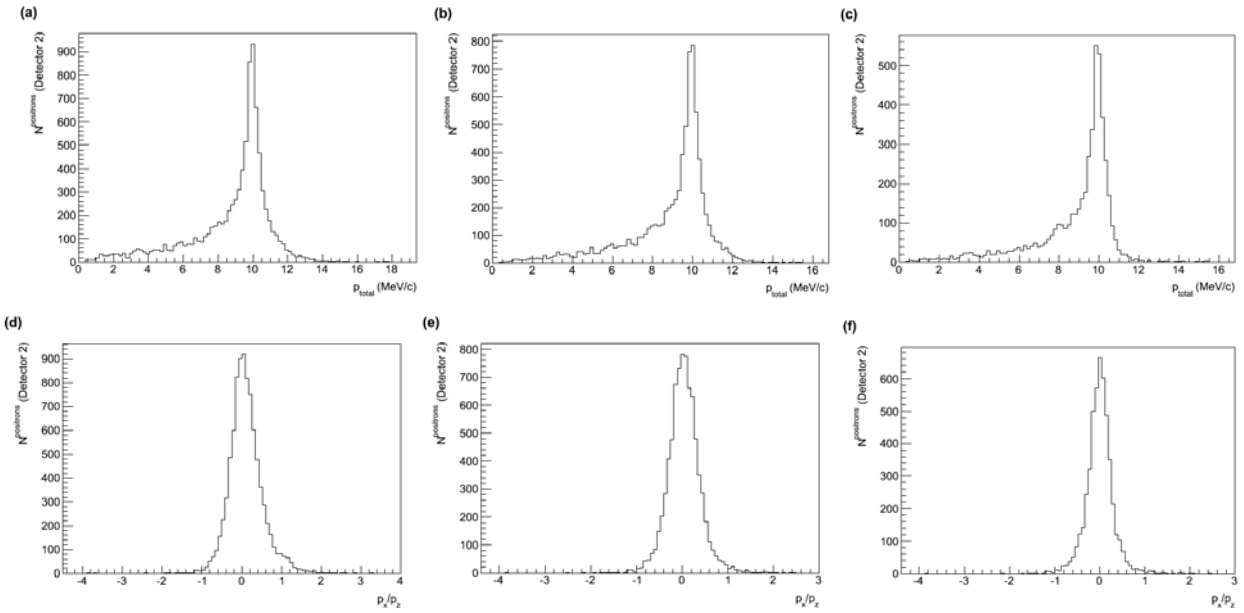

FIG. 7. Momentum distributions after wedge for (a) no cut, (b) tan (Θ_{init}) ≤ 0.5, (c) tan (Θ_{init}) ≤ 0.2; P_x/P_z or tan (Θ_{final}) distributions after the wedge for (d) no cut, (e) tan(Θ_{init}) ≤ 0.5, (f) tan(Θ_{init}) ≤ 0.2.

Table 2: Effect of limiting initial positron angle on final positron sample

	All $\tan(\Theta_{init})$	**$\tan(\Theta_{init}) \leq 0.5$**	**$\tan(\Theta_{init}) \leq 0.2$**
#e+ before wedge	50314	33610	18189
#e+ after wedge	8963	7838	4920
$\sigma(P_{tot})$ (MeV/c)	1.05	1.05	0.8
$\sigma(P_{tot})/P_{peak}$ (%)	4.6	4.6	3.4
$\sigma(P_x/P_z)$	0.43	0.36	0.31
$\sigma(\Theta_{final})$	23.3°	19.8°	17.2°

The widths of the momentum distributions in Table 2 were calculated from the FWHM of the peaks, which is more representative of the widths than the statistical RMS, which are biased by the tails. Restriction of positron production angles to $\tan(\Theta_{init}) \leq 0.5$, or 26.6° reduces the positron sample after the wedge by 33%, does not improve the momentum resolution of the final sample, and improves the width of the angular spread after the wedge by 18%. Restriction of positron production angles to $\tan(\Theta_{init}) \leq 0.2$, or 11.3° reduces the positron sample by 45%, while reducing the momentum spread of the positrons after the wedge by 24% and reducing the angular spread by 26%. Collimation of the initial positron production angles at the production target can be designed to optimize positron rates and spreads after the wedge. Furthermore the tails of the positron momentum distribution can be reduced by improving the shielding.

B. Comparison between collimator and wedge

A more conventional method to obtain nearly monoenergetic positrons is through the use of a collimator, i.e. a momentum slit. In this case the positrons with parameters outside of a chosen range are rejected. Simulations of the yields of positrons using a collimator instead of a wedge were made with the layout shown in F 8. The trajectories of positrons originating at the target are shown, with some passing through the slit in the collimator shield to the virtual detector, shown in green.

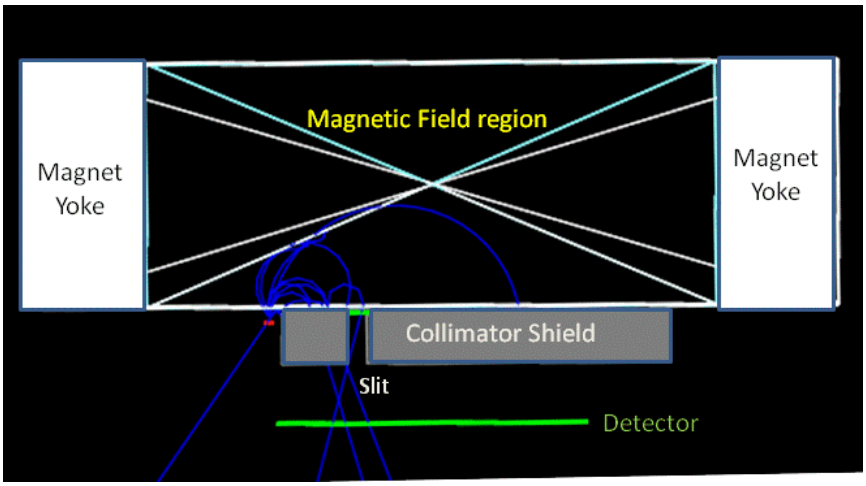

FIG. 8. Layout of dipole magnet and collimator for simulation.

The results are shown in Fig. 9 for 10 MeV/c positrons, and in Table 3 for 2 MeV/c, 5 MeV/c, and 10 MeV/c positrons. The sample of positrons was generated by the same number of electrons on the same target as for the dipole plus wedge simulations.

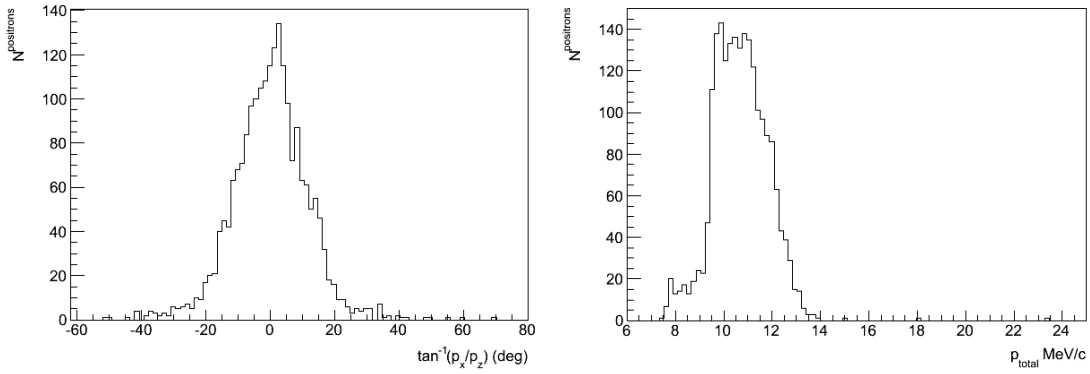

FIG. 9. Results for collimators. The plot on the left shows the distributions in angle in x-z plane and the plot on the right shows the momentum distribution for 10 MeV/c.

The results using a dipole plus wedge (Table 1) are compared with the results for the collimator in Table 3. The momentum peak widths and angular spreads are similar, but the positron yields are ~4 to 10 times higher for the wedge than for the collimator. The result can be understood because the wedge makes use of higher-energy positrons, while the collimator rejects them.

Table 3: Results for collimator, and positron yield ratio

P_{Final} (MeV/c)	P_{RMS}/P_{Final} (%)	Θ_{RMS} (°)	$\#e^+$ After Coll (Y_{Coll})	Y_{Wedge}/Y_{Coll}
2	9.5	15.6	410	7.2
5	11.4	13.4	1167	10.4
10	10.3	11.7	2102	4.2

C. Summary of this section

The results of the simulations have shown that a dipole plus a wedge can be used to reduce a broad positron momentum spectrum to RMS spreads of approximately 15%, 8%, and 4% in the selected momentum ranges around 2 MeV/c, 5 MeV/c, 10 MeV/c, respectively. Furthermore, the yields of positrons in the selected momentum ranges for a dipole plus wedge are greater than the yields for a conventional dipole plus collimator by a factor of ~7, 10, and 4 for the three momentum ranges studied. The method can be used to select other nearly monoenergetic positron momenta by varying the magnetic field strength and the wedge dimensions. In general, low-Z wedge materials produce sharper momentum distributions and less multiple Coulomb scattering. We have presented results for Be wedges. Liquid hydrogen or liquid helium would produce better results, but would require cryogenics and containment vessels. Another attractive wedge material is lithium hydride (LiH) because it is a low-Z solid with a long radiation length.

V. GAMMA RAY PRODUCTION

A. Concept

We present a method of producing gammas by annihilation in flight of nearly monoenergenic positrons against electrons in a converter target. A discussion of methods of producing gamma rays by annihilation in flight was presented at the IPAC10 conference [9]. This produces a sample of gammas in which the gamma energy spectrum is enhanced near the incident positron energy. The energy spectrum of gammas produced by positron annihilation in flight has a higher proportion of gammas in the desired energy region than the bremsstrahlung spectrum resulting from electrons impinging on a high-Z target. The bremsstrahlung spectrum falls off monotonically with gamma energy. Appendix A contains the relevant physics and kinematics that are needed to understand the benefits of positron annihilation in flight.

When a beam of positrons impinges on material, a number of processes take place in addition to annihilation in flight. Positrons lose energy and scatter in the converter material, which tends to smear the gamma ray energies. For thick targets, some of the positrons are stopped and annihilate at rest, producing the characteristic pair of 0.511 MeV gammas. The material and the thickness of the converter can be optimized to produce the best combination of rate and resolution of the gamma ray energy spectra for the intended application. A description of the factors affecting the choice of converters is presented next, followed by results of simulations of a number of materials and thicknesses.

A low-Z converter material minimizes the production of photons by bremsstrahlung and angular spread due to multiple Coulomb scattering off the nuclei. The lowest-Z material is pure hydrogen, either as a gas or liquid (boiling point -253^{o}C). While hydrogen offers the best performance, it has some disadvantages. In practice, hydrogen must be contained in a vessel, which adds higher-Z material to the annihilation target. In the simulations performed here, we show results for pure liquid hydrogen, without including window materials. Two other commonly used low-Z materials are lithium hydride (LiH, melting point 692^{o}C) and beryllium (Be, melting point 1297^{o}C).

Larger target thickness improves the conversion efficiency of positrons into photons, but adds to the angular spread of the positrons and photons and degrades the energy of the positrons, contributing to larger photon energy spread. Any positrons that stop and annihilate at rest contribute a significant isotropic 0.511 MeV background. We investigated the yields and backgrounds from both thick and thin converter targets. We concluded that LiH offered the best combination of rate and background. Three thicknesses of LiH converters were studied: 1mm, 10mm, and 100mm. We also present simulation results for hydrogen and beryllium, for comparison.

The method used can produce various photon energy ranges for a variety of applications. We present simulation results for production of photons near 10 MeV. The results are presented for a configuration that includes the positron production subsystem and the dipole plus wedge subsystem that have been described earlier as well as the photon production components.

B. Photon Energy Spectra from Simulations of Positrons Impinging on a Converter

We have performed simulations of a pencil beam of a million 10 MeV/c positrons striking lithium hydride converters of 1 mm, 10 mm, and 100 mm thickness, and also liquid hydrogen and beryllium converters, for comparison. We have also accepted gammas that emerge from the converter within two angular ranges – within 0.1 radians and within 0.5 radians. The energy spectra for LiH are shown in Fig. 10.

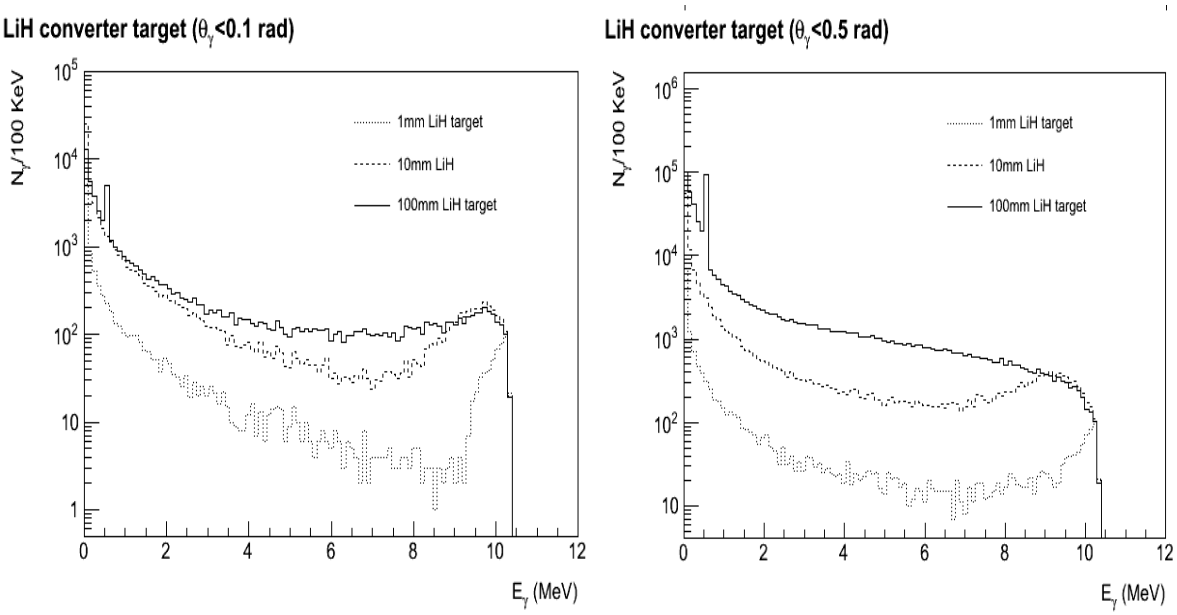

FIG. 10. Gamma energy spectra for LiH converters of thickness 1mm, 10 mm, and 100 mm. (left) gammas with angles less than 0.1 radians, (right) gammas with angles less than 0.5 radians.

The following characteristics are noted. There is a rapid falloff from the low energy peak near zero energy for all three converter thicknesses until the emergence of the full energy annihilation peak near 10 MeV. For the 1 mm converter there is a pronounced valley between the peaks. As the thickness of the converter increases, the overall number of gammas increases, but the depth of the valley between the bremsstrahlung and the maximum energy peak decreases. For the thinner converter**,** the positrons lose a smaller fraction of their initial energy before annihilating, while for the thickest converter (100 mm LiH) the positrons lose energy before annihilating, and the gamma ray energy spectrum tends to approach a constant up to the maximum energy. In addition, there is a noticeable peak at 0.511 MeV, due to those positrons that come to rest before annihilating. For the 1 mm and 10 mm converters there are not a significant number of annihilations at rest.

The ratio of the number of events in the ~10 MeV peak to the valley is about 2 for the 100 mm converter, 7 for the 10 mm converter, and about 45 for the 1 mm converter. While the intensities of the ~10 MeV peaks are nearly the same (200 gammas per 100 KeV) for the 10 mm and 100 mm converters, the peak value for the 1 mm converter is ~90 gammas per 100 KeV, about a factor of 2 less yield.

The results of the simulations for LiH with an enlarged acceptance angle for the gamma rays are shown in F. One can see that the number of events has increased by about a factor of 2. For the 100 mm converter there is no longer a peak near 10 MeV, just a shoulder. We also note that the low energy gammas, below ~1 MeV, may be eliminated by hardening the gamma ray spectrum by inserting a high-Z thin foil after the converter.

A numerical summary of the results for LiH is presented in Table 4. The numbers of events for 1.0×10^6 incident positrons are shown, for the total energy range and for 2 MeV wide energy ranges. The intended energy range is from 8 to 10 MeV. The number of events in the 8 to 10 MeV range varies from 502 to 7398, depending on the converter thickness and the angular range, corresponding to 5×10^{-4} to 7.4×10^{-3} per incident positron.

Table 4: Summary of gamma production from LiH converters for various thicknesses and angular ranges. The integer values represent the numbers of gammas produced in the energy ranges shown per million incident positrons. The gamma peak characteristics, shown as decimal numbers, represent the relative number of gammas in the targeted energy range (8 to 10 MeV) compared to the total number of gammas produced and compared to the next lower energy interval (6 MeV to 8 MeV).

Material	**LiH**	**LiH**	**LiH**	**LiH**	**LiH**	**LiH**
Thickness	**1 mm**	**10 mm**	**100 mm**	**1 mm**	**10 mm**	**100 mm**
Angle	**< 0.1 rad**	**< 0.1 rad**	**< 0.1 rad**	**< 0.5 rad**	**< 0.5 rad**	**< 0.5 rad**
Energy Range						
0 to 10 MeV	9,813	54,274	52,274	13,870	122,746	460,762
8 to 10 MeV	502	3,044	3,151	785	6,462	7,398
6 to 8 MeV	87	684	2,040	298	3,554	12,863
4 to 6 MeV	200	1,155	2,463	411	4,071	20,664
2 to 4 MeV	430	2,793	4,153	689	6,811	31,007
0 to 2 MeV	8,606	46,679	40,616	11,706	102,079	390,047
Gamma Peak Characteristics						
(8 to 10MeV)/Total	0.051	0.056	0.061	0.057	0.053	0.016
(8 to 10)/(6 to 8)	5.77	4.45	1.54	2.63	1.82	0.58

Results for Beryllium and Hydrogen Converters

Thicknesses of beryllium and hydrogen converters were chosen that provide the same number of electrons per cm^2 as the values for the three LiH converters. The gamma spectra for a beryllium converter are shown in Fig. 11, also produced from 1.0×10^6 incident positrons. The curves are qualitatively similar to those for LiH.

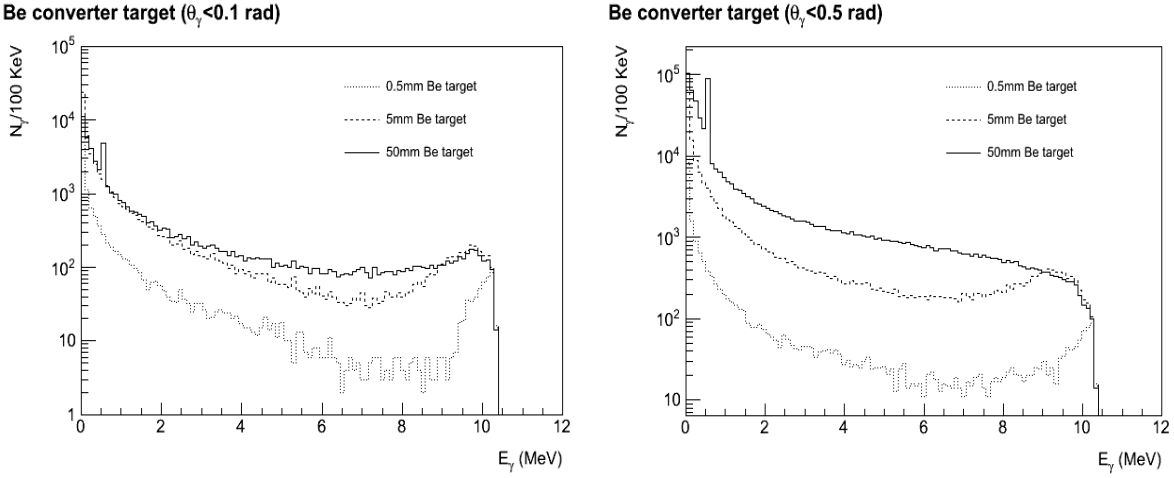

FIG. 11: Gamma energy spectra for Be converters, (left) for gamma angles within 0.1 radians, (right) for gamma angles within 0.5 radians.

A similar table for Be converters is shown in Table 5.

Table 5: Summary of gamma production from Be converters for various thicknesses and angular ranges. The integer values represent the numbers of gammas produced in the energy ranges shown. The gamma peak characteristics, shown as decimal numbers, represent the relative number of gammas in the targeted energy range (8 to 10 MeV) compared to the total number of gammas produced and compared to the next lower energy interval (6 MeV to 8 MeV).

Material	Be	Be	Be	Be	Be	Be
Thickness	0.5 mm	5 mm	50 mm	0.5 mm	5 mm	50 mm
Angle	< 0.1 rad	< 0.1 rad	< 0.1 rad	< 0.5 rad	< 0.5 rad	< 0.5 rad
Energy Range						
0 to 10 MeV	11,788	55,677	50,546	16,818	146,656	486,622
8 to 10 MeV	321	2320	2389	611	6202	7228
6 to 8 MeV	98	741	1705	332	3815	12704
4 to 6 MeV	237	1248	2205	455	4507	18765
2 to 4 MeV	587	3124	4239	908	8707	31415
0 to 2 MeV	10,370	47,985	39,774	14,328	123,148	416,264
Gamma Peak Characteristics						
(8 to 10MeV)/Total	0.027	0.042	0.047	0.036	0.042	0.015
(8 to 10)/(6 to 8)	3.28	3.13	1.4	1.84	1.63	0.57

The results for liquid hydrogen converters are shown in Fig. 12. As expected, the production of gammas in the 8 MeV to 10 MeV region is greater in relation to the 6 MeV to 8 MeV region. These results are for pure hydrogen and do not include the hydrogen container walls and other non-hydrogen material.

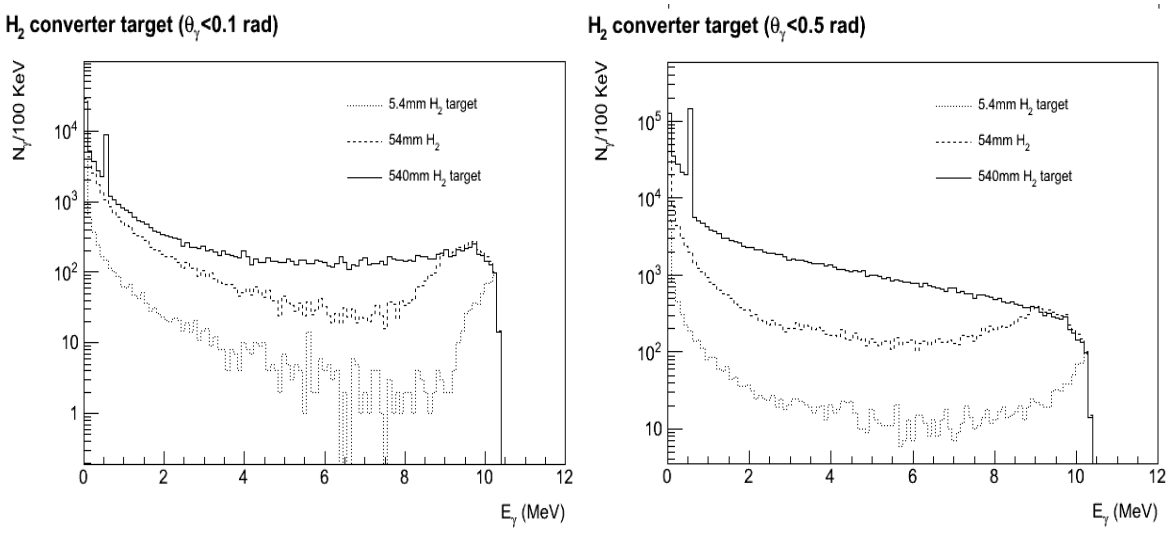

FIG. 12. Gamma energy spectrum for liquid hydrogen converters, (left) for gamma angles within 0.1 radians, (right) for gamma angles within 0.5 radians. Variations are due to statistical fluctuations.

Table 6: Summary of gamma production from H_2 converters for various thicknesses and angular ranges. The integer values represent the numbers of gammas produced in the energy ranges shown. The gamma peak characteristics, shown as decimal numbers, represent the relative number of gammas in the targeted energy range (8 to 10 MeV) compared to the total number of gammas produced and compared to the next lower energy interval (6 MeV to 8 MeV).

Material	**H_2**	**H_2**	**H_2**	**H_2**	**H_2**	**H_2**
Thickness	**5.4 mm**	**54 mm**	**540 mm**	**5.4 mm**	**54 mm**	**540 mm**
Angle	**< 0.1 rad**	**< 0.1 rad**	**< 0.1 rad**	**< 0.5 rad**	**< 0.5 rad**	**< 0.5 rad**
Energy Range						
0 to 10 MeV	7,212	52,063	70,814	10,039	96,079	500,881
8 to 10 MeV	301	3,141	3,600	532	5655	6,778
6 to 8 MeV	47	558	2,777	252	3026	12,522
4 to 6 MeV	112	790	2,862	277	2877	19,970
2 to 4 MeV	265	2,001	4,481	444	4453	33,983
0 to 2 MeV	6,309	45,347	56,855	8,352	79,803	42,7383
Gamma Peak Characteristics						
(8 to 10MeV)/Total	0.0417	0.0603	0.0508	0.0529	0.0588	0.0135
(8 to 10)/(6 to 8)	6.4	5.63	1.3	2.11	1.87	0.54

VI. SUMMARY

Design concepts have been presented for a system to produce beams of nearly monoenergetic gamma rays tunable in the energy range around 10 MeV. The gamma rays are produced in the forward direction by annihilation in flight of nearly monoenergetic positrons. The positrons are produced by an electron beam and target system optimized for positron production in the useful kinematic region. Following the positron production section is the "dipole plus wedge" monochromator, in which the positrons are bent 180° in a uniform magnetic field to disperse their momenta, after which a wedge absorber selectively reduces their momentum spread to a narrow range.

The system emphasized in this paper is optimized for the production of a ~10 MeV photon beam. That choice of energy is not intrinsic to the system design but is driven by the application of detecting fissionable material while minimizing the amount of induced radioactivity and the radiation dose in the scanned object.

Simulations of the positron production from 75 MeV electrons bombarding a W target and gammas produced by annihilation of positrons in flight in several different converter materials and thicknesses produced the following representative results:

- For the selection of positrons produced within $\tan(\Theta) \leq 0.2$, the ratio of positrons to incident electrons is about 5×10^{-3}.
- For a LiH converter of thickness 10 mm, the ratio of gammas within the targeted energy range (8 MeV to 10 MeV) is about 3×10^{-3} per incident positron.
- For this condition the ratio of gammas in the targeted energy range to the total number of gammas is 0.05 and the ratio of gammas in the 8 to 10 MeV peak to the adjacent 6 to 8 MeV range is about 6.

In summary, if one assumes that all of the positrons produced within $\tan(\Theta) \leq 0.2$ and emerging from the wedge impinge on the converter, the rate of useful gammas per incident electron is about 1.5×10^{-5}. Therefore 10^{15} electrons are required on target to produce 1.5×10^{10} useful gammas. An electron flux of 10^{15} electrons per second represents an average beam current of 0.16 mA; the corresponding electron beam power at 75 MeV is 12 kW.

APPENDIX A: FORMULAE FOR TWO-PHOTON ANNIHILATION OF ELECTRON-POSITRON PAIRS

The following constants are used:

- Electron mass, m=0.511 MeV;
- Classical electron radius r_e=2.818x10^{-13} cm, r_e^2=7.941x10^{-26} cm^2

The process $e^+ + e^- \to 2\gamma$ is described by two Feynman diagrams (Fig.A-1).

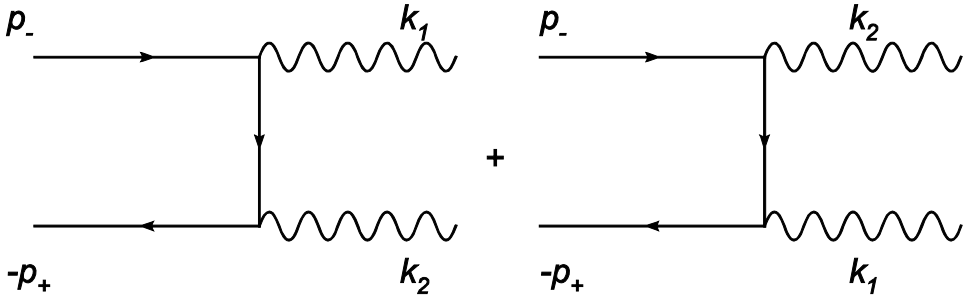

FIG A-1: Feynman diagrams for electron-positron annihilation.

Mandelstam invariants are defined as:

$$s = (p_- + p_+)^2 = (k_1 + k_2)^2,\ t = (p_- - k_1)^2,\ u = (p_- - k_2)^2,$$

where $p_+(p_-)$ is the 4-momentum of an initial electron (positron), and $k_{1,2}$ are 4-momenta of the final gammas. Energy-momentum conservation requires that $s + t + u = 2m^2$.

The differential cross section in terms of Mandelstam invariants valid in an arbitrary reference frame is:

$$\frac{d\sigma}{d(-t)} = 8\pi r_e^2 \frac{m^2}{s(s-4m^2)}\left\{\frac{1}{4}\left(\frac{u-m^2}{t-m^2}+\frac{t-m^2}{u-m^2}\right)-\left(\frac{m^2}{t-m^2}+\frac{m^2}{u-m^2}\right)^2-\left(\frac{m^2}{t-m^2}+\frac{m^2}{u-m^2}\right)\right\}$$

The variable *t* is within the range corresponding to 0 and 180 degrees of photon emission:

$$-\frac{s}{2}-\frac{1}{2}\sqrt{s(s-4m^2)} \le t-m^2 \le -\frac{s}{2}+\frac{1}{2}\sqrt{s(s-4m^2)}.$$

Integrating the cross section with respect to t, and dividing by two to account for identical photons in the final state, we obtain a total cross section for electron-positron annihilation as a function of Mandelstam s, where τ=s/m^2:

$$\sigma_{annih} = \frac{2\pi r_e^2}{\tau^2(\tau-4)}\left[(\tau^2+4\tau-8)\ln\frac{\sqrt{\tau}+\sqrt{\tau-4}}{\sqrt{\tau}-\sqrt{\tau-4}}-(\tau+4)\sqrt{\tau(\tau-4)}\right],$$

Note that to obtain a formula for the photon rate from annihilation, the above cross section should be multiplied by two, since two gammas are produced per event, $\sigma_\gamma = 2\sigma_{annih}$.

Consider electron and positron beams with momenta along the z-axis. Four momenta $p=(p_0;p_x,p_y,p_z)$, are defined as: $p_+ = (E_p;0,0,p_p), p_- = (E_e;0,0,p_e),\ k_1 = E_\gamma(1;\sin\theta\cos\varphi,\sin\theta\sin\varphi,\cos\theta)$, where

E_γ and θ are the energy and an angle of a produced gamma , $E_{p(e)} = \sqrt{p_{p(e)}^2 + m^2}$. Same (opposite) signs of p_p and p_e correspond to collinear (head-on) collisions.

Mandelstam variables in terms of lab observables are:

$$s = (p_+ + p_-)^2 = 2m^2 + 2E_pE_e - 2p_pp_e,$$
$$t = (p_- - k_1)^2 = m^2 - 2p_-k_1 = m^2 - 2E_eE_\gamma + 2p_eE_\gamma\cos\theta,$$
$$u = (p_+ - k_1)^2 = m^2 - 2p_+k_1 = m^2 - 2E_pE_\gamma + 2p_pE_\gamma\cos\theta$$

Using energy-momentum conservation, $s + t + u = 2m^2$, the photon energy is related to its emission angle as

$$E_\gamma = \frac{m^2 + E_pE_e - p_pp_e}{E_p + E_e - (p_p + p_e)\cos\theta} .$$

Depending on the relative signs of the colliding particle momenta, the maximum (or minimum) of the produced gamma energy corresponds to θ=0 or 180°. In a special case of opposite momenta that are equal in magnitude, the produced gammas are monoenergetic with energy equal to the incoming beam energy, $E_\gamma=E_p=E_e$.

In the limit of the electron target at rest (E_e=0.511MeV, p_e=0), the above formula becomes

$$E_\gamma = \frac{m}{1 - \frac{p_p}{E_p + m}\cos\theta} ,$$

providing one-two-one correspondence between the energy and the emission angle of the gamma.

To evaluate the photon (energy) spectrum in the lab, we need a Jacobian,

$$dt = \left(\frac{dt}{dE_\gamma}\right)dE_\gamma, \qquad \frac{dt}{dE_\gamma} = 2\frac{(E_pp_e - E_ep_p)}{(p_e + p_p)}.$$

For angular distribution of the photons in the lab, another Jacobian is needed:

$$dt = \left(\frac{dt}{d\cos\theta}\right)d\cos\theta, \ \frac{dt}{d\cos\theta} = 2\frac{(E_pp_e - E_ep_p)(E_eE_p - p_ep_p + m^2)}{[E_p + E_e - (p_p + p_e)\cos\theta]^2}$$

The cross section that is differential in a chosen variable can be obtained from the expression for $\frac{d\sigma}{d(-t)}$ using the Jacobians, namely:

$$\frac{d\sigma}{dE_\gamma} = \frac{d\sigma}{dt}\left(\frac{dt}{dE_\gamma}\right) = \frac{d\sigma}{dt}\cdot\frac{2(E_pp_e - E_ep_p)}{(p_e + p_p)}; \frac{d\sigma}{dcos\theta} = \frac{d\sigma}{dt}\left(\frac{dt}{dcos\theta}\right) = \frac{d\sigma}{dt}\cdot\frac{2(E_pp_e - E_ep_p)(E_eE_p - p_ep_p + m^2)}{[E_p + E_e - (p_p + p_e)\cos\theta]^2}.$$

These formulas give, respectively, distributions of the produced photons over energies and polar angles, while distribution over the azimuthal angle φ is uniform.

Particular features of the annihilation gamma spectra from *relativistic* beams that are relevant for the considered application include natural focusing of produced gammas within an opening angle of $\Delta\theta = \pm 1/\gamma$ and peaking in the gamma energy spectrum within the range $\frac{\Delta E_\gamma}{E_{\gamma;max}} = \frac{1}{2\gamma}$, where $\gamma = \frac{E_p}{m}$.

Let us consider a numerical example. For a target electron at rest (E_e=0.511 MeV, p_e=0) and a positron beam energy E_p=9.5 MeV the energy of produced gammas varies between the minimum and maximum values that are uniquely defined by the emission angle of the gamma: $E_{\gamma;min}$=0.25 MeV; $E_{\gamma;max}$=9.77MeV.

The energy vs angle dependence in the forward region is shown in Fig. A-2, where one can see that for the forward opening angles within about ±0.25 rad, the energies of the gammas exceed 6 MeV, resulting in photofission in fissionable materials. The corresponding total cross section for gamma production is σ_γ=0.83x10^{-25} cm^2. The energy spectrum of annihilation gammas (Fig.A-3) shows strong peaking in energy near the endpoint.

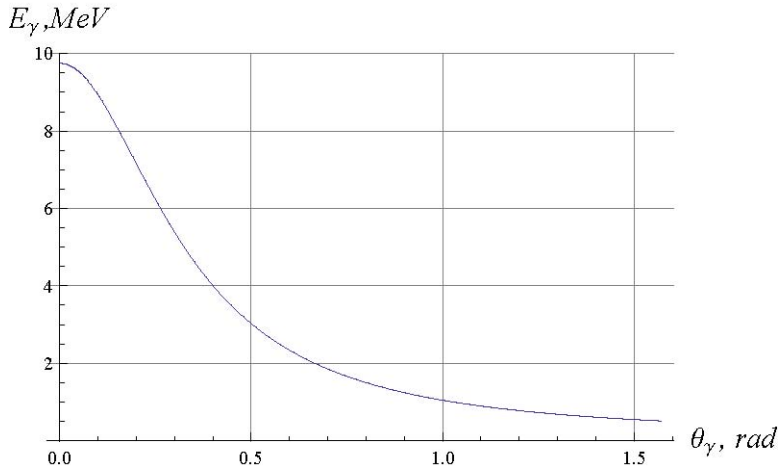

FIG. A-2. Energy vs angle of annihilation gammas in the forward region for 9.5 MeV positron beam incident on an electron target at rest.

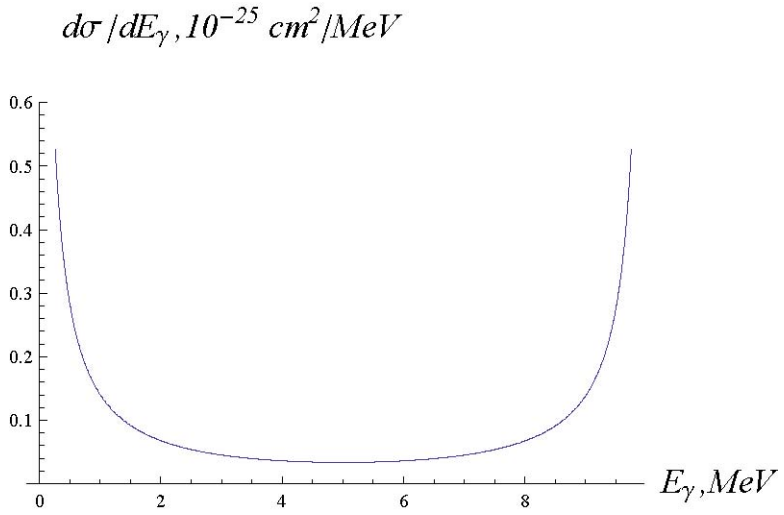

FIG A-3: Energy spectrum of annihilation gammas for 9.5 MeV positron beam incident on an electron target at rest.

Let us estimate a total yield of gammas that is defined by the product of luminosity and the above cross section. The luminosity is given by:

$$L = r_p \rho_e h,$$

where r_p is the number of incident positrons per unit time, ρ_e is the volume density of target electrons, and h is the target thickness. For a 0.5 mm-thick graphite target we obtain

$$\rho_e \cdot h = 6.6\text{x}10^{23}\text{cm}^3\text{x}0.05\text{cm} = 3.3\text{x}10^{22}\text{electrons/cm}^2.$$

A positron beam of $r_p=10^{14}$ positrons/s incident on the above target will result in a luminosity $L=3.3\text{x}10^{38}\text{cm}^{-2}\text{s}^{-1}$ and the yield of annihilation gammas

$$L\cdot\sigma_\gamma = 2.6\text{x}10^{12}\ \text{Hz}.$$

Appendix A Reference:

"Quantum Electrodynamics" by V. B. Berestetsky, E. M. Lifshitz , L. P. Pitaevskii , Published by Butterworth-Heinemann; 2 edition (January 15, 1982).

APPENDIX B: DESIGN AND CALIBRATION OF WEDGES

The sizes and shapes of Be wedges for producing nearly monoenergetic positrons are determined by the following procedure. An initial estimation of the thickness and angle of the wedge is based on the expected momentum loss of positrons passing through the material of the wedge. The final result is obtained by simulation, as described below.

The layout of the dipole magnet and the wedge, with representative trajectories for the 10 MeV/c calibrations, is shown in Fig. B-1.

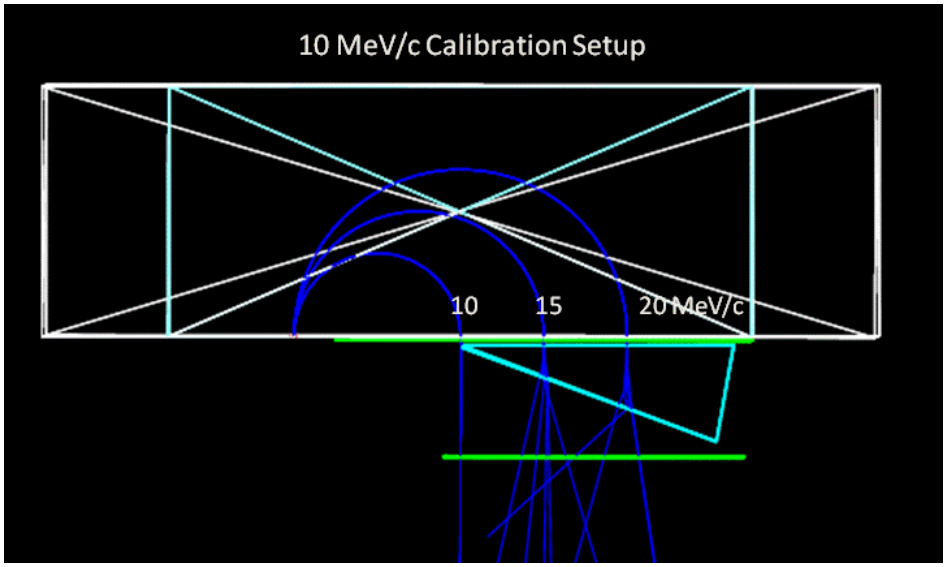

FIG. B-1. G4beamline event display for a calibration setup for 10 MeV/c**.** The blue trajectories are for positrons. The green trajectories shown are gammas produced by positrons interacting in the wedge. In this figure there were 5 positrons generated at each momentum.

Positrons were generated using G4beamline at 10, 15, and 20 MeV/c. For a magnetic field strength of 1.333 T, the radius of curvature in the field is 25 mm for 10 MeV/c and 50 mm for 20 MeV/c. The trajectory of the 10 MeV/c positrons just misses the tip of the wedge, and so emerges from the magnet at 10 MeV/c. Other positrons lose momentum as a function of position along the wedge. When the wedge is properly designed, each positron emerges from the wedge with momentum near 10 MeV/c, depending on statistical variations in the momentum loss. Scattering also takes place, as shown in Fig. B-1.

The results of the calibration are shown in Fig. B-2. As can be seen, there is a spike at 10 MeV/c, which is due to the 10 MeV/c incident positrons. The distribution around the spike is due to the 15 and 20 MeV/c positrons, also peaking at 10 MeV/c. The individual distributions for the 15 and 20 MeV/c positrons are shown in Fig. B-2 (b) and (c), respectively. The peaks for 15 and 20 MeV/c line up well at 10 MeV/c, with statistical RMS spreads of 1.5 and 1.9 MeV/c, respectively. The alignment of the peaks at 10 MeV/c indicates that the momentum loss is proportional to the thickness of the wedge, so that a triangular wedge is a suitable shape. The resulting wedge, as designed using Be, has a 60 mm base and is 160 mm long.

The same procedure can be used to design wedges to produce other desired final momenta, or for use of other wedge materials.

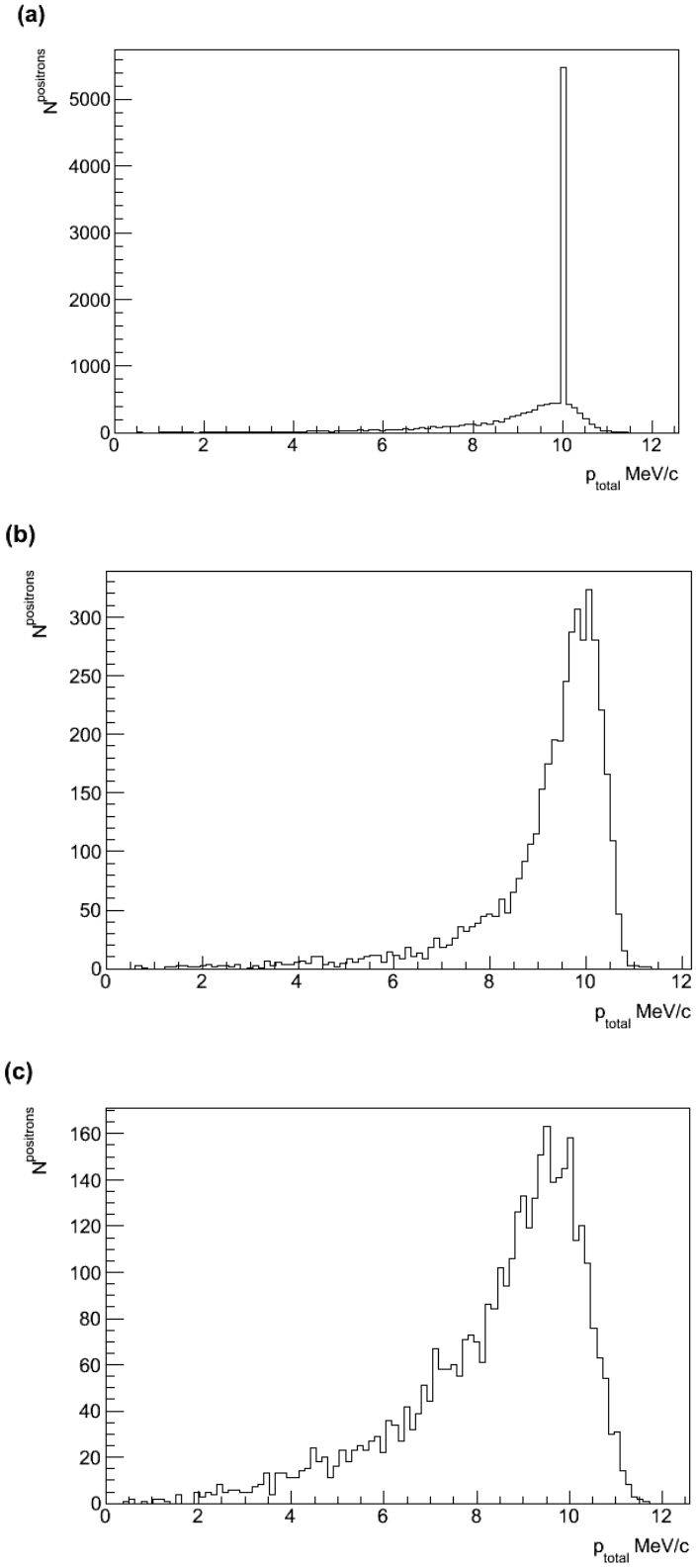

FIG. B-2: Calibration results for 10 MeV/c final momentum. (a) Final momentum spectrum after wedge for 10, 15, and 20 MeV/c incident momenta, (b) momentum distribution for 15 MeV/c incident momentum, (c) momentum distribution for 20 MeV/c incident momentum.

REFERENCES

[1] R. Mosley, Science and Global Security **1**, 303 (1990); *Report on the Workshop on the Role of the Nuclear Physics Research Community in Combating Terrorism,* Eds: J. Moss et al., DOE Report No. DOE/SC-0062 (July 2002); J.L. Jones et al., Nucl. Inst. Meth. Phys. Res. Ser. B **261**, 326 (2007); T. Gozani, IEEE Trans. Nucl. Sci. **56**, 736 (2009).

[2] J.T. Caldwell et al., Phys. Rev. C 21, 1215 (1980).

[3] A. Veyssiere et al, Nucl. Phys. A 199, 45 (1973).

[4] B.L. Berman, S.C. Fultz, Rev. Mod. Phys. 47, 713 (1975).

[5] S. S. Dietrich, B. L. Berman, Atomic Data and Nuclear Data Tables, 38, 199 (1988).

[6] C. Yoshikawa, R. Abrams, A. Afanasev, C. Ankenbrandt, K. Beard, D. Neuffer, "Positron production for a Compact Tunable Intense Gamma Ray Source", Proceedings of IPAC10, paper MOPEA045. http://accelconf.web.cern.ch/accelconf/IPAC10/papers/mopea045.pdf

[7] R. Abrams, C. Ankenbrandt, and C. Yoshikawa, "Quasi-Monoenergetic Positrons Using Dipole and Wedge", Proceedings of IPAC10, paper MOPEA044. http://accelconf.web.cern.ch/accelconf/IPAC10/papers/mopea044.pdf

[8] T. J. Roberts, http://g4beamline.muonsinc.com/

[9] A. Afanasev, R. Abrams, C. Ankenbrandt, K. Beard, C. Yoshikawa, " Quasi-monoenergetic photon source based on electron-positron in-flight annihilation", Proceedings of IPAC10, paper MOPEA043. http://accelconf.web.cern.ch/accelconf/IPAC10/papers/mopea043.pdf